Applied Surface Science 410 (2017) 585–592

Contents lists available at ScienceDirect

Applied Surface Science

journal homepage: www.elsevier.com/locate/apsusc

Full Length Article

Comparison of interface structure of BCC metallic (Fe, V and Nb) films on MgO (100) substrate

J.L. Du[a,1], L.Y. Zhang[b,1], E.G. Fu[a,*], X. Ding[b,*], K.Y. Yu[c,*], Y.G. Wang[a], Y.Q. Wang[d], J.K. Baldwin[d], X.J. Wang[e], P. Xu[f]

[a] State Key Laboratory of Nuclear Physics and Technology, School of Physics, Peking University, Beijing 100871, PR China
[b] State Key Laboratory for Mechanical Behavior of Materials, Xi'an Jiaotong University, Xi'an, 710049, PR China
[c] Department of Materials Science and Engineering, China University of Petroleum, Beijing 102249, PR China
[d] Experimental Physical Sciences Directorate, Los Alamos National Laboratory, Los Alamos, NM 87544, USA
[e] State Key Laboratory of Advanced Optical Communication Systems and Networks, Peking University, Beijing 100871, PR China
[f] Department of Chemistry, Harbin Institute of Technology, Harbin, Heilongjiang, 150001, PR China

ARTICLE INFO

Article history:
Received 22 July 2016
Received in revised form
22 September 2016
Accepted 20 October 2016
Available online 26 October 2016

Keywords:
Interface structure
Match type
HRTEM
First-principle calculation

ABSTRACT

This study systematically investigates the interface structure of three body-centered-cubic (BCC) metallic (Fe, V and Nb) films grown on MgO(100) substrates through experiments and simulations. Orientation relationships of their interfaces with the different lattice mismatches exhibit cube-on-cube configurations. The misfit dislocations at these three interfaces exhibit different characteristics. High resolution TEM (HRTEM), combined with first principle calculations, demonstrates the O-atop match type between metal atoms and MgO substrates for the first time. The fundamental mechanism in determining the interface configuration is discussed in terms of the work of separation and delocalization of atomic charge density.

1. Introduction

Heterophase interfaces are widely studied due to their ability of enhancing the radiation tolerance of materials [1–8]. Owing to high density heterophase interfaces, materials with multiple phases or precipitates in radiation environments usually exhibit evenly distributed voids or He bubbles with small size (sometimes even undetectable) and thereby alleviate radiation hardening and swelling [9–13]. Thus, tailoring the density of interfaces is becoming one of the most effective ways to enhance radiation tolerance and success has been achieved in many nanomaterials.

Nevertheless, the atomic structure of interfaces has been increasingly concerned as it affects the sink strength of the interfaces significantly. Extensive studies suggest the width of defect-denuded zone (DDZ), which is commonly used to characterize the sink ability of interface, is closely correlated to the interface structure [14]. Nucleation, migration and clustering of interfacial vacancies and interstitials are strongly dependent on the structure and configuration of interfaces [15,16]. For instance, high angle grain boundaries with low vacancy formation energies can act as powerful vacancy sinks, while other grain boundaries (e.g. $\Sigma 3$ boundaries) where vacancy formation energies are comparable to those in the neighboring crystalline material are less effective [17,18].

BCC metals are promising candidates for future nuclear applications as they show much better swelling resistance than the face-centered-cubic (FCC) counterparts. Ferritic-martensitic steels (F/M steel), nano-ferritic alloys (NFA), and in particular, oxide-dispersion-strengthened (ODS) steels have attracted global interests for the development of next generation nuclear materials. It has been reported that the BCC iron/oxide heterophase interfaces within ODS alloys are expected to acquire increased sink ability if appropriate interface structure can be obtained. Hence systematic knowledge on the formation mechanisms of the BCC metal/oxide interface is required for the design of radiation resistant alloys such as ODS steels. Related works have shown that irradiation induced defects in the BCC alloy/oxide systems are very mobile and annihilate in an effective manner [19–26].

* Corresponding authors.
E-mail addresses: efu@pku.edu.cn, fuengang@gmail.com (E.G. Fu), dingxd@mail.xjtu.edu.cn (X. Ding), kyyu@cup.edu.cn (K.Y. Yu).
[1] J.L. Du and L.Y. Zhang contributed equally to the work.

http://dx.doi.org/10.1016/j.apsusc.2016.10.117
0169-4332/

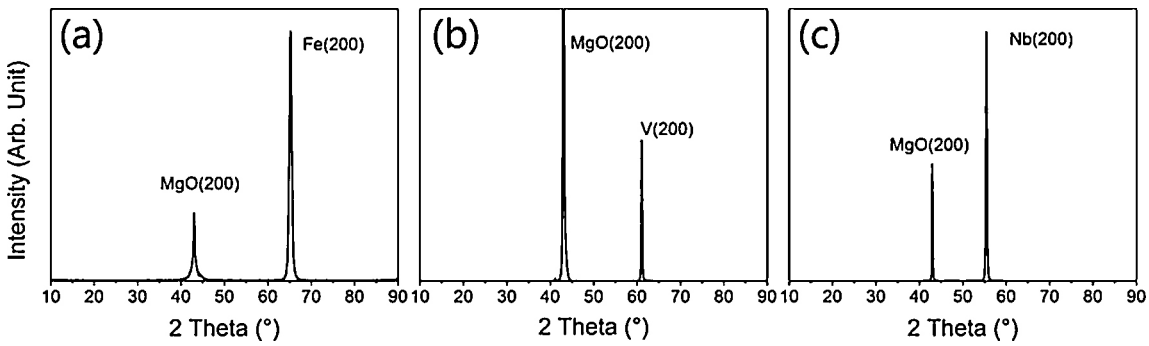

Fig. 1. XRD θ-2θ patterns of Fe, V and Nb films deposited on MgO(100) substrates by e-beam evaporation. The preferential planes of Fe, V and Nb films on MgO(100) plane are Fe(100), V(100) and Nb(100), respectively.

Our previous work has shown that the work of separation, together with substrate orientation and lattice mismatch, determines the orientation relationships between BCC metal films and MgO substrates, and the work of separation is the dominant factor [27]. Others have reported that BCC metals, such as Nb [27], Fe [28,29], V [30], Ta [31], and Cr [32], grow on MgO(100) substrate with a typical orientation relationship of metal(100)[011]//MgO(100)[001], that is, the metal(100) plane is rotated by 45° around the metal[100] axis. In addition, the match type(O-atop or Mg-atop) of metal/MgO interface might also affect the chemical stability of the interface. Simulations have suggested that the metal/MgO interface follows the O-atop match type [33–35] although direct experimental evidences are rarely reported. In this study, three typical BCC metals are deposited on single crystal MgO(100) substrates with negative lattice mismatched (Fe/MgO), coherent (V/MgO), and positive lattice mismatched (Nb/MgO) interfaces. We identify the interface atomic structure and find direct experimental evidence of O-atop match type which is consistent with first principle calculations. Possible interface formation mechanisms are discussed.

2. Experiments

Fe, V and Nb films were deposited on MgO(100) substrates by electron beam evaporation with the substrate temperature of 500 °C, 700 °C and 950 °C, respectively. Single crystal MgO substrates were etched in 85% o-phosphoric acid (H_3PO_4) for 45 s followed by rinsing in the deionized water. After that, they were loaded into a vacuum chamber immediately to minimize surface roughening and hydroxide formation. The substrates were exposed by electron cyclotron resonance microwave plasma operated at 200W and 2×10^{-4} Pa O_2 for 30 min to remove adventitious carbon contamination on the surface [36,37].

Van der Merwe suggested that when the film thickness is larger than the critical thickness given by Mathews' equation, the lattice mismatch is accommodated by forming interface misfit dislocations [22–24]. Moreover, it is reported that as the film thickness increases, higher crystalline quality of the film is achieved resulting from the decrease of auto-doped defect concentration in films [38,39]. All film thicknesses were about 180 nm to guarantee the formation of misfit dislocation network in interface and high crystalline quality. The film thickness was measured in TEM by tilting the sample to follow MgO[001] zone axis.

XRD experiments were performed using a PYNalitic X-Pert3 X-ray powder diffractometer with $\lambda_{CuK\alpha 1}$ = 0.15406 nm. The rocking curve experiments were performed by Philips X'PERT-MRD X-ray diffractometer using the same wavelength at room temperature. The cross-sectional TEM specimens were prepared by grinding and low energy (3.5 keV) Ar ion milling. A FEI Tecnai F30 transmission electron microscope working at 300 kV with a field-emission gun was used to observe the microstructures of the as-deposited films. Images were recorded by a Gatan UltraScan model 994 CCD camera with the image size of 2048 × 2048 pixels.

3. Results

Fig. 1(a–c) show XRD θ–2θ patterns of Nb, V and Fe films on MgO(100) substrates, respectively. Strong reflections of metal(200) are observed, indicating the Nb, V and Fe films are strongly texture with (100) planes in parallel with MgO(100) plane. The crystalline quality of Fe, V and Nb films was investigated by the full width at half maximum (FWHM) of rocking curves, which are primarily used to determine the mean spread (range) in orientation of the different out-of-plane crystalline domains of a perfect crystal with mis-orientation. Table 1 shows the values of FWHM of Fe(200), V(200) and Nb(200) rocking curves. It is found that the FWHM values of Fe, V and Nb films are $FWHM_{Fe}$ = 0.378°, $FWHM_V$ = 0.243°, and $FWHM_{Nb}$ = 0.438°, respectively, indicating that the V film has the highest crystalline quality, while the Nb film has the lowest one.

Fig. 2 shows the TEM micrographs of metal(100)/MgO(100) interface. Fig. 2a is the bright-field TEM micrograph of Fe(100)/MgO(100) taken at MgO[001] zone axis. Inset is the corresponding selected area electron diffraction (SAD) pattern and shows Fe[011]//MgO[001] and Fe(100)//MgO(100). This orientation relationship is consistent with the XRD results. Fig. 2b is the HRTEM micrograph of Fe(100)/MgO(100) interface structure. Fe(100) plane is rotated 45° around the Fe[100] axis and the interface roughness is smaller than 3 nm. The misfit dislocations which are formed due to the lattice mismatch between Fe(011) and MgO(020) plane were labeled by the red "⊥" in Fig. 2b and the average dislocation spacing is measured as ~4.9 nm. The Burgers vector of the misfit dislocation was determined as **b** = Fe[0$\bar{1}$1] shown in inset of Fig. 2b.

Fig. 2c and e show the interface structure of V and Nb films on MgO(100) substrates. The preferential orientation relationships investigated by both XRD and SAD pattern are the same as that of Fe/MgO(100). Also, it is noted that the V[100] and Nb[100] are parallel to the MgO[100]. Fig. 2d is the HRTEM micrograph of V/MgO(100) interface which is observed along MgO[001] direction, showing that the interface of V/MgO is coherent. However, some dislocations are observed in the MgO substrate, labeled by red "⊤" or "⊥". Fig. 3f shows the HRTEM micrograph of Nb/MgO(100) interface. The misfit dislocations are labeled by "⊤", with the Burg-

Table 1
The FWHM values of rocking curves for Fe(200), V(200) and Nb(200) planes.

	Fe(200)	V(200)	Nb(200)
Lattice mismatch δ	−6.1%	1.5%	10.3%
FWHM	0.378°	0.243°	0.438°

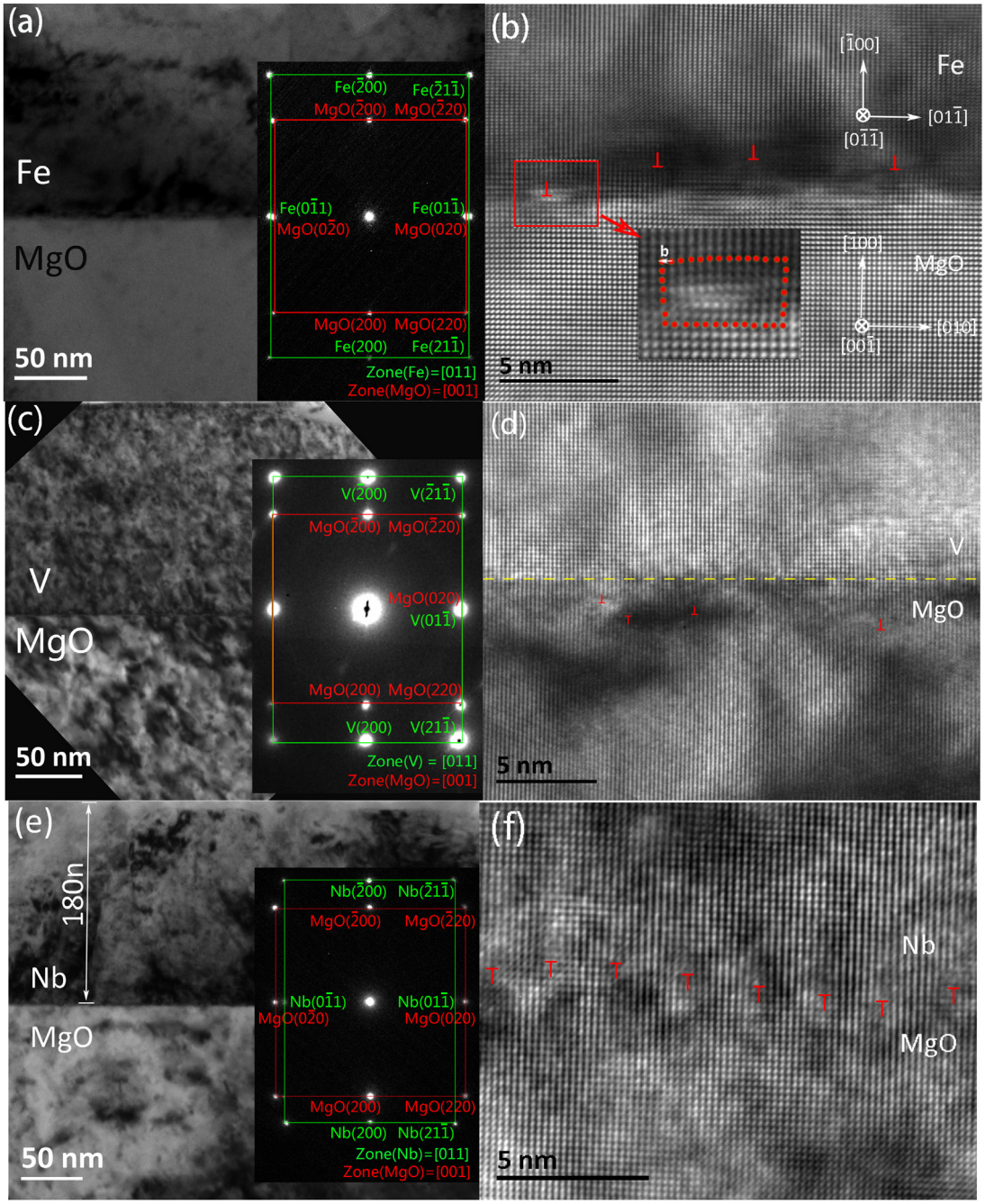

Fig. 2. Bright-field TEM micrographs of (a) Fe(100)/MgO(100), (c) V(100)/MgO(100), and (e) Nb(100)/MgO(100), insets are the corresponding selected area diffraction (SAD) patterns respectively. (b), (d) and (f) are the corresponding HRTEM micrograph observed along the MgO[001] zone axis, and the inset in (b) is the enlarged filtered image showing the Burgers vector of a misfit dislocation. (For interpretation of the references to colour in the text, the reader is referred to the web version of this article.)

ers vector **b** = 1/2Nb[01$\bar{1}$] and the average dislocation spacing is measured as ~1.9 nm.

4. Discussion

4.1. Interface structure in Fe/MgO, V/MgO and Nb/MgO

The Fe, V and Nb films were grown on the MgO(100) substrate by electron beam evaporation with the substrate temperature of 500 °C, 700 °C and 950 °C, respectively. Fe, V and Nb all have bcc structure with lattice parameter: a_{Fe} = 0.2806 nm, a_V = 0.3027 nm, a_{Nb} = 0.3307 nm, while MgO has a fcc structure with lattice parameter a_{MgO} = 0.4217 nm.The lattice mismatch between Fe film and MgO substrate was investigated here. Lattice mismatch (δ) can be expressed by Eq. (1) [40,41]:

$$\delta = 2(d_f - d_s)/(d_f + d_s) \quad (1)$$

where d_s and d_f are the lattice spacing of the substrate and the thin film, respectively. If one assumes the interface misfit dislocation is fully accommodated by the relaxation of the in-plane lattice mismatch, the average interface dislocation spacing can be given by [19]:

$$L = \frac{b}{\delta} \quad (2)$$

where b is the magnitude of the Burgers vector of misfit dislocation parallel to the interface, as shown in Fig. 2b. The Burgers vector of

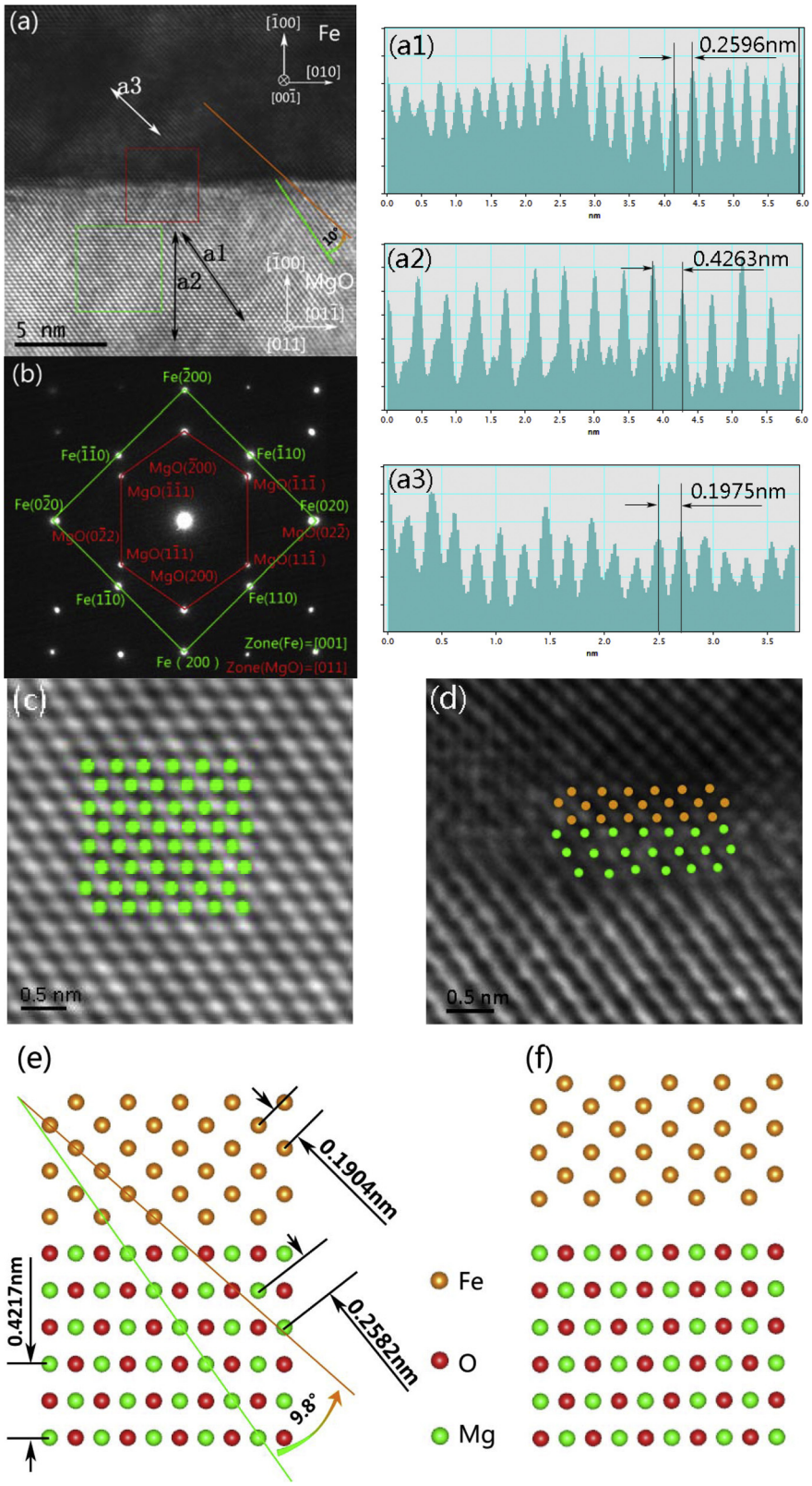

Fig. 3. (a) HRTEM micrograph of Fe(100)/MgO(100) viewed along the MgO[011] axis; (b) The corresponding selected area diffraction (SAD) pattern; (a1), (a2) and (a3) shows the intensity of the HRTEM spots along the line a1, a2 and a3 in Fig. 3a, and the average atom spacing is calculated as 0.2596 nm, 0.4263 nm and 0.1975 nm, respectively. (c) Enlarged image of the region labeled by the green box in Fig. 3a. (d) Enlarged image of the region labeled by the red box in Fig. 3a. (e) and (f) are the O-atop and Mg-atop match type calculated by first principle calculations, respectively. (For interpretation of the references to colour in this figure legend and text, the reader is referred to the web version of this article.)

Table 2
The lattice mismatch and dislocation spacing of Fe/MgO, V/MgO and Nb/MgO interfaces. a_s and a_f are the lattice parameter of substrate and metal films, where subscript s and f represent substrate and film, respectively. δ is the lattice mismatch from the direction along MgO[010] axis. Dislocation spacing is the average distance of misfit dislocations measured by HRTEM.

	a_f (nm)	a_s (nm)	$d_{f(011)}$ (nm)	$d_{s(020)}$ (nm)	δ	Burgers vector	dislocation spacing
Fe	0.2806	0.4217	0.1984	0.2109	−6.1%	Fe [0$\bar{1}$1]	4.9 nm
V	0.3027	0.4217	0.2140	0.2109	1.5%	*	*
Nb	0.3307	0.4217	0.2338	0.2109	10.3%	Nb [01$\bar{1}$]	1.9 nm

*: no misfit dislocation observed due to coherent interface.

the misfit dislocation was determined as **b** = 1/2Fe[0$\bar{1}$1] by drawing circuit around the dislocation. Corresponding lattice mismatch is $\delta = 2(d_{Fe(011)} - d_{MgO(020)})/(d_{Fe(011)}+d_{MgO(020)}) = -6.1\%$. Thus the calculated average dislocation spacing of misfit dislocations is $L = b/\delta = 3.3$ nm. In comparison, the value measured from the HRTEM image is ~4.9 nm. Previous study shows that the semi-coherent interface releases strain by forming misfit dislocations and the interface is characterized by coherent regions separated by periodically spaced misfit dislocations [32,40,41]. This difference could be due to the co-existence of residual stress at the coherent regions and misfit dislocations [4,27,42].

The interface coherencies of V(100)/MgO(100) interface and Nb(100)/MgO(100) are also studied. The lattice mismatch of V/MgO(100) between V(011) and MgO(020) is $\delta = 2(d_{V(011)} - d_{MgO(020)})/(d_{V(011)}+d_{MgO(020)}) = 1.5\%$. It is well known that the interface is likely to form the coherent structure when the lattice mismatch is smaller than 5.0%. For the lattice mismatch of 1.5% in V/MgO(100), the coherent interface has been observed under HRTEM [33,34] and no misfit dislocation along the interface is found as they are well matched. However, some edge dislocations are observed in the bulk MgO substrate, and this may be due to the motivation of misfit dislocations [34]. The calculated spacing between misfit dislocations of Nb/MgO(100) interface is $L = b/\delta = 2.4$ nm, based on the lattice mismatch of $\delta = 2(d_{Nb(011)} - d_{MgO(020)})/(d_{Nb(011)}+d_{MgO(020)}) = 10.3\%$ calculated by using E.q. (1). This calculated value of dislocation spacing is larger than the measured value ~1.9 nm and it may be due to the fact that the distribution of misfit dislocations is non-uniform and the observed regions has a higher density of misfit dislocations.

On the other hand, the location of edge misfit dislocations are investigated by HRTEM in Fe/MgO(100) and Nb/MgO(100) systems. The misfit dislocations are located at Fe side on the interface of Fe film grown on MgO(100) substrate, while the misfit dislocations are located at MgO side on the Nb/MgO(100) interface, that is, the Fe/MgO interface shows the positive misfit dislocations while the Nb/MgO interfaces show negative misfit dislocations. This corresponds with the negative lattice mismatch and positive lattice mismatch. It is well known that the misfit dislocations should be located at the side with smaller interplanar spacing. The interplanar spacing of Fe(011) planes is $d_{Fe[011]} = 0.1984$ nm, while the MgO(020) is $d_{MgO(020)} = 0.2109$ nm, thus the misfit dislocations of Fe/MgO(100) interface are located at the Fe film side, showing positive misfit dislocations. While for Nb/MgO interface, the interplanar spacing of Nb(011) planes is $d_{Nb(011)} = 0.2338$ nm, which is large than $d_{MgO(020)} = 0.2109$ nm, thus the misfit dislocations are located at the MgO side. The differences are listed in Table 2.

4.2. Crystalline quality of Fe, V and Nb films

The crystalline quality of Fe, V and Nb films is investigated by the FWHM values of Fe(200), V(200) and Nb(200) rocking curves and the results are listed in Table 1. The FWHM values of Fe, V and Nb films are $FWHM_{Fe} = 0.378°$, $FWHM_V = 0.243°$, and $FWHM_{Nb} = 0.438°$, respectively, indicating that the V film has the best crystalline quality, while the Nb film has the worst one. Also, the lattice mismatch of these three interfaces is listed as Table 1, and it is found that the order of the magnitude of lattice mismatch is $\delta_{Nb/MgO} > \delta_{Fe/MgO} > \delta_{V/MgO}$. Our previous study shows the degree of Nb crystalline perfection in Nb(110)/Al_2O_3 (11$\bar{2}$0) system is higher than that in Nb(110)/MgO(111) and the reason is due to its smaller lattice mismatch in Nb (110)/Al_2O_3(11$\bar{2}$0), which may lead to smaller residual strain around interface. In the current case, the observation shows that V/MgO interface has the smallest lattice mismatch, and thus has the smallest amount of residual strain. As a result, the V/MgO interface has the highest crystalline perfection in these three films.

4.3. Orientation relationships between BCC metal film and MgO substrate

XRD results (Fig. 1) show that all these three films exhibit the same preferential out of plane on MgO(100) substrate, i.e., metal(100)//MgO(100). Combined with the SAD pattern (Fig. 2a,c,e), it is found that all these three metals follows the same orientation relationships, that is, metal(100)//MgO(100), metal[011]//MgO[001] and metal[01$\bar{1}$]//MgO[010]. The first principle calculation through the coherent models was used to understand the fundamental mechanisms for forming the interface configuration. The coherent periodic slab model [40,43] in current calculation represents an interface as a sandwich of semi-infinite crystal layers. This sandwich model is constituted by MgO, metal and vacuum layer. For a given sandwich model, the thickness of vacuum layer was set to be 15 Å. MgO substrate was kept in the strain-free state while the lattice constant of metal film was changed to construct the coherent interfaces. In addition, two types of coherent interface configurations were considered, where metal atoms sit on the top of either O or Mg atoms, denoted as O-atop and Mg-atop, respectively.

The built sandwich model was then relaxed by using the Atomistix ToolKit (ATK) software package in order to optimize the crystal structure and calculate the electronic properties of the interface between metal (Fe, V and Nb) and MgO [44]. Spin-polarized local density approximation (LSDA) with the Perdew–Zunger parameterization was used as the exchange and correlation function [45,46]. Single zeta plus polarization (SZP) basis set was selected for the electron wave function. A cutoff energy of 75 Hartree and a Monkhorst–Pack k-mesh of 7 × 7 × 1 were used for all calculations. Lattice parameters and atomic coordinates were fully relaxed until the maximum force on each atom was less than 0.05 eV $Å^{-1}$. The similar building process of the interface structure models can be found elsewhere [27].

Work of separation (W_{sep}) is the fundamental factor to characterize the bonding strength of the metal/oxide interface, which is defined as the reversible work needed to separate the interface into two free surfaces and is usually written as [47]

$$W_{sep} = (E_{MgO} + E_{metal} - E_{total})/S \quad (3)$$

where E_{metal} is the energy of single metal (Fe, V or Nb) slab and is obtained by maintaining the parallel strains of metal(Fe, V or

Table 3
Structure parameters and calculation results of coherent Fe/MgO(100), V/MgO(100) and Nb/MgO(100) models. Detailed information of the six models are given as follows: orientation relationships (ORs), interface mismatch (δ'), lattice mismatch along two directions (δ_l,δ_m), interface distance (x, given in Å), work of separation (W_{sep}, given in eV Å^{-2}).

	Model	δ'	(ε_l, ε_m)	Match type	x	W_{sep}
Fe/MgO	Fe(100)//MgO(100)	6.5%	(6.7%, 6.7%)	O-atop	2.1	0.18
	Fe[01$\bar{1}$]//MgO[001]			Mg-atop	2.1	0.13
	Fe[01$\bar{1}$]//MgO[010]					
	Fe(110])//MgO(100)	4.2%	(−2.1%, 6.7%)	O-atop	2.6	0.08
	Fe[00$\bar{1}$]//MgO[011]			Mg-atop	2.6	0.07
	Fe[$\bar{3}$31]//MgO[01$\bar{1}$]					
	Fe(111)//MgO(100)	6.2%	(−9.8%, 2.6%)	O-atop	2.1	0.12
	Fe[312]//MgO[031]			Mg-atop	2.6	0.05
	Fe[121]//MgO[01$\bar{2}$]					
V/MgO	V(100)//MgO(100)	0.3%	(−0.3%, −0.3%)	O-atop	2.1	0.21
	V[011]//MgO[001]			Mg-atop	3.3	0.03
	V[01$\bar{1}$]//MgO[010]					
	V(110)//MgO(100)	2.9%	(0.3%, 6.5%)	O-atop	2.7	0.07
	V[$\bar{1}$10]//MgO[011]			Mg-atop	2.7	0.07
	V[001]//MgO[01$\bar{1}$]					
	V(111)//MgO(100)	10%	(0.3%, 1.7%)	O-atop	2.4	0.07
	V[1$\bar{1}$2]//MgO[018]			Mg-atop	2.4	0.07
	V[$\bar{1}$10]//MgO[0$\bar{1}$0]					
Nb/MgO	Nb(100)//MgO(100)	9.8%	(9.8%, 9.8%)	O-atop	2.3	0.17
	Nb[0$\bar{1}$1]//MgO[010]			Mg-atop	2.8	0.02
	Nb[011]//MgO[001]					
	Nb(110)//MgO(100)	4.3%	(1.0%, 7.6%)	O-atop	2.5	0.13
	Nb[001]//MgO[0$\bar{1}$1]			Mg-atop	2.4	0.09
	Nb[1$\bar{1}$0]//MgO[011]					
	Nb(111)//MgO(100)	2.9%	(4.0%, 6.7%)	O-atop	2.5	0.08
	Nb[$\bar{1}$10]//MgO[001]			Mg-atop	3.4	0.04
	Nb[11$\bar{2}$]//MgO[010]					

Nb) slab, E_{MgO} is the energy of single MgO slab, E_{total} is the total energy of the whole interface, S is the area of interface. Two preset cutoff values of interface mismatch (δ') and lattice strain (ε_l) are used to reduce the number of interface configuration models. The lattice strain is the strain of metal film along a given direction, e.g., $\varepsilon_l = (a' - a)/a$, where a' and a are the lattice constants after and before deformation along l direction. The interface mismatch (δ') refers to the strain required to make two unit cells form coherent structure, and is defined as

$$\delta' = 1 - (2\Omega)/(S_A + S_B) \quad (4)$$

where Ω represents the overlap area of unit cell with the match cell area of S_A in the film and the match area of S_B in the substrate [40]. It should be noted that the δ' is commonly used to describe two plane mismatch of heterointerface, different from the lattice mismatch δ in one direction. All the calculated results are listed in Table 3. It is found that metal(100)//MgO(100), metal[011]//MgO[001] and metal[01$\bar{1}$]//MgO[010] have the largest work of separation. Therefore, work of separation can be used as the criterion to predict the interface orientation relationships of Fe/MgO, V/MgO and Nb/MgO interfaces.

4.4. O-atop or Mg-atop model?

In order to further understand the interface crystallography, the first principle calculation was used to investigate the preferential orientations and interface chemistry. Previous experimental studies of BCC metal films deposited on MgO reported that BCC metal atoms usually sit on the top of either O or Mg atoms [27,34], thus there could be two different simulation match types between metal atoms and MgO substrate, i.e., O-atop type and Mg-atop type. It is essential to clarify the match type of BCC metal films and MgO substrate to further understand the interface chemistry. The bonding mechanism of the metal/oxide interfaces are widely studied by the first principle calculations and most of these studies support the view that the metal film atoms are sit on the O atoms of MgO substrate, i.e., O-atop type [34,35]. However, to our best knowledge, very few experimental studies verify the simulation results based on bonding mechanism of the metal/oxide interfaces. In order to verify the O-atop match type experimentally, the HRTEM micrograph of Fe/MgO(100) interface viewed along the MgO[011] zone axis shown in Fig. 3. The Fig. 3a and b show the bright HRTEM micrograph and corresponding SAD pattern viewed along the MgO[011] zone, showing the orientation relationships between Fe thin film and single MgO substrate. Fig. 3(a1),(a2) and (a3) shows the intensity of the HRTEM spots along the line a1, a2 and a3 in Fig. 3a, and the average atom spacing is calculated as 0.2596 nm, 0.4263 nm and 0.1975 nm, respectively. Also,we note that the angle between the line a1 and line a3 is about 10°, just as Fig. 3a shows. Fig. 3c and d show the enlarged images of the region labeled by the green and red box in Fig. 3a, respectively. Fig. 3e and f show the simulated atomic configurations of O-atop model and Mg-atop model observed along the MgO[011] direction. Comparison of the HRTEM micrograph (Fig. 3c) and the simulated MgO lattice structure (Fig. 3e) shows that the average atom spacing along a1, a2 and a3 line are 0.2596 nm, 0.4263 nm and 0.1975 nm, which is similar to the simulated value 0.2582 nm, 0.4217 nm and 0.1974 nm, respectively. The angle between the line a1 and line a3 is about 10°, which is similar to the simulated 9.8°, just as Fig. 3e shows. We thus deduce that the high light spots can be thought to be the Mg atoms or the O atoms. Considering the scattering factor of atom to electrons, the O atoms are too weak to scatter electrons and form dark spots in the HRTEM paragraph. Thus the dark spots in Fig. 3c are the Mg lattice-sites (labeled by green dots), while the high light spots can be thought to be the O lattice-sites. Then, the atomic structure of Fe/MgO interface is characterized in Fig. 3d. The Mg lattice-sites are labeled by green spots at the MgO side of the Fe/MgO interface while the orange spots are Fe atoms. In this way, it is defined that Fe atoms are located just a half distance between two Mg lattice sites, which is the O atom site. The O-atop type model is found to be the actual match type of metal/MgO interface.

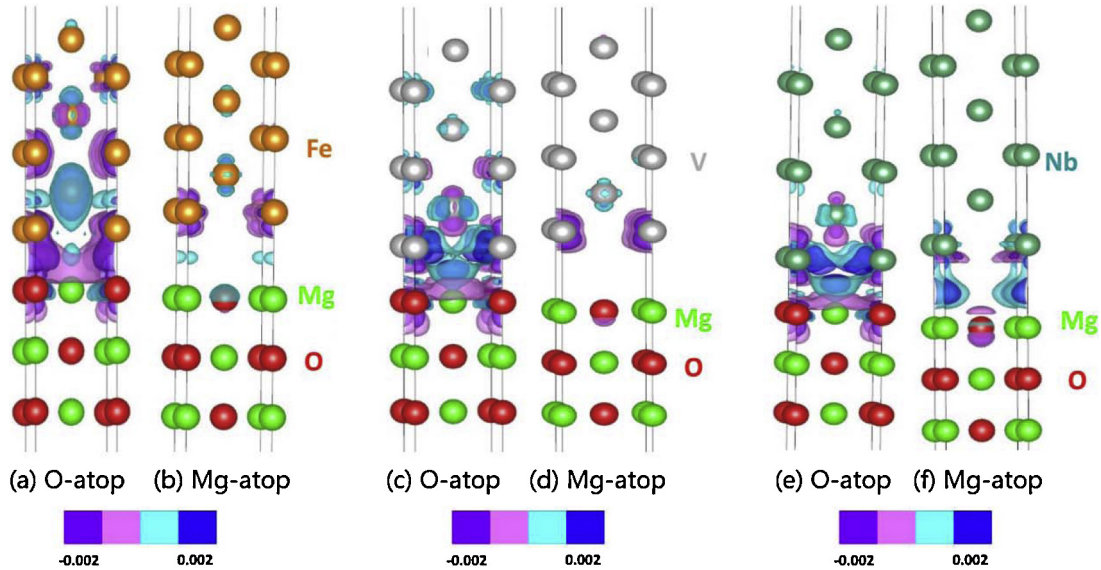

Fig. 4. Electron density difference maps of Fe(100)/MgO(100), V(100)/MgO(100) and Nb(100)/MgO(100) interface, with the indication of atoms that are near to the interface. The isosurface value for the violet color (electrons accumulation) is −0.002 electrons/Å^3, and for the blue color (electrons depletion) is 0.002 electrons/Å^3. Fe, V, Nb, O, Mg atoms are indicated by different colors: Fe (orange), V (gray), Nb (dark green), O (red), Mg (green). (For interpretation of the references to colour in this figure legend, the reader is referred to the web version of this article.)

4.5. Difference in electron density

First principle calculations of Fe/MgO, V/MgO and Nb/MgO interfaces (Table 3) show that the calculated interface configuration with the biggest work of separation is consistent with experimental observations. To further understand the work of separation, it is essential to investigate the interface chemistry, and therefore the bonding information for BCC/MgO(100) interfaces. The bonding information can be visualized by delocalization of atomic charge density. The electron density difference ($\Delta\rho$) maps exhibit the strength of bond between BCC metal atoms and O atoms of MgO substrate, and the results are shown in Fig. 4, where $\Delta\rho = \rho_{A/B}$-$(\rho_A + \rho_B)$, $\rho_{A/B}$ is the self-consistent electron density of whole relaxed metal/substrate interface structure, ρ_A and ρ_B are the electron densities of isolated metal and substrate slabs having the same atomic positions in the interface structure.

For all these three systems, film metal atoms (Fe, V and Nb) lose electrons, and O atoms gain electrons, as the blue and violet color shown. This means that electrons are transferred from Fe, V and Nb films to substrate along the interface and redistributed. The transfer mainly happens between the six Fe layers, five V layers and three Nb layers that are close to the interface. Furthermore, the transfer of electrons in V(100)/MgO(100) is stronger than that in Fe(100)/MgO(100) and Nb(100)/MgO(100), which indicates that ionic bonds in V/MgO interface are stronger than that in Fe/MgO and Nb/MgO systems. The transfer of electrons can be understood by electronegativity and bond length. Electronegativity is a chemical property that describes the tendency of an atom or a functional group to attract electrons (or electron density) towards itself [48]. The most commonly used method of the electronegativity calculation is originally proposed by Linus Pauling and the scale of electronegativity of Fe, V, Nb and O is 1.83, 1.63, 1.60 and 3.44, respectively [49]. The interface distance of Fe/MgO, V/MgO and Nb/MgO is 2.1 Å, 2.1 Å and 2.3 Å, respectively, which can be used to describe the bond strength of interface. This study shows that V/MgO interface exhibits stronger transfer of electrons than Fe/MgO interface and it should be due to the larger electronegativity difference of V/MgO than Fe/MgO interface. Also, the reason why the electron redistribution of V/MgO interface is stronger than Nb/MgO interface is due to the smaller interface distance in V/MgO interface. On the other hand, it is found that the O-atop type models of all Fe/MgO, V/MgO and Nb/MgO interface exhibit stronger bond strength than Mg-atop models, which also indicates that O-atop model is the actual way of combination between BCC metal atom and MgO substrate. As a conclusion, the strength of ion bonds between film metal atoms and substrate O ions is found to be the fundamental factor to determine the interface configurations between BCC metal films and MgO substrates.

5. Conclusion

Fe, V and Nb films were deposited by e-beam evaporations on MgO(100) substrates. Their interfaces exhibit cube-on-cube configuration despite that the lattice mismatch between metals and substrate is negative, negligible and positive respectively. The preferential orientations relationships are metal(100)//MgO(100), metal[011]//MgO[001] and metal[01$\bar{1}$]//MgO[010]. The HRTEM reveals the misfit dislocations are distributed along the metal/MgO interfaces to accommodate the in-plane lattice mismatch between metal films and MgO substrates. Fe/MgO(100) interface shows the positive edge dislocations with the Burgers vector **b** = 1/2Fe[0$\bar{1}$1], while the Nb/MgO interface shows the negative edge dislocations with the Burgers vector **b** = 1/2Nb[01$\bar{1}$]. The V/MgO interface exhibits the coherent structure due to well-matched lattice. The O-atop model of metal atoms and MgO substrate is experimentally verified by HRTEM. Combined with the first principle calculations, the strength of bonds along interface is found to be the fundamental factor to determine the interface configurations between BCC metal thin films and MgO substrates.

Acknowledgements

The authors thank Dr. M.J. Zhuo and Mr. L.P. You for insightful discussions. Thin film deposition and XRD experiments were supported by the user proposal (U2014B0112) approved by the Center for Integrated Nanotechnologies (CINT), a US Department of Energy, Office of Basic Energy Sciences user facility at Los Alamos National Laboratory (LANL). The TEM analysis portion of this work was supported by Electron Microscopy Laboratory of Peking University. This work was supported by ITER special funding with

award number of 2015GB121004 from Ministry of Science and Technology, and by Natural Science Foundation of China with Award Number of 11375018 and 11528508. E.F. appreciates the support from The Recruitment Program of Global Youth Experts in China, and the Instrumental Analysis Fund of Peking University, and X.D. appreciates the support of NSFC (51320105014, and 51321003, 51231008). K.Y. appreciates the financial support from NSFC (51501225) and CUPB (2462015YQ0602).

References

[1] W.Z. Han, M.J. Demkowicz, N.A. Mara, E.G. Fu, S. Sinha, A.D. Rollett, Y.Q. Wang, J.S. Carpenter, I.J. Beyerlein, A. Misra, Design of radiation materials via interface engineering, Adv. Mater. 25 (2013) 6975–6979.
[2] E.G. Fu, J. Carter, G. Swadener, A. Misra, L. Shaok, H. Wang, X. Zhang, Size dependent enhancement of helium ion irradiation tolerance in sputtered Cu/V nanolaminates, J. Nucl. Mater. 385 (2009) 629–632.
[3] E.G. Fu, A. Misra, H. Wang, L. Shao, X. Zhang, Interface enabled defects reduction in helium ion irradiated Cu/V nanolayers, J. Nucl. Mater. 407 (2010) 178–188.
[4] E.G. Fu, Y.Q. Wang, M. Nastasi, Mechanisms for ion-irradiation-induced relaxation of stress in mosaic structured Cu thin films, J. Phys. D 45 (2012) 495303.
[5] S.J. Zheng, I.J. Beyerlein, J.S. Carpenter, K. Kang, J. Wang, W.Z. Han, N.A. Mara, High-strength and thermally stable bulk nanolayered composites due to twin-induced interfaces, Nat. Commun. 4 (2013) 1696.
[6] A. Misra, M.J. Dekmowicz, X. Zhang, G.G. Hoagland, The radiation damage tolerance of ultra-high strength nanolayered composites, JOM 59 (2007) 62–65.
[7] K.Y. Yu, Y. Liu, E.G. Fu, Y.Q. Wang, M.T. Myers, H. Wang, L. Shao, X. Zhang, Comparisons of radiation damage in He ion and protron irradiated immiscible Ag/Ni nanolayers, J. Nucl. Mater. 440 (2013) 310–318.
[8] Y. Chen, L. Jiao, S. Sun, M. Song, K.Y. Yu, Y. Liu, M. Kirk, M. Li, H. Wang, X. Zhang, In situ studies of radiation induced crystallization in Fe/α-Y_2O_3 nanolayers, J. Nucl. Mater. 452 (2014) 321–327.
[9] E.G. Fu, H. Wang, J. Carter, L. Shao, Y.Q. Wang, X. Zhang, Fluence-dependent radiation damage in helium (He) ion-irradiated Cu/V multilayers, Philos. Mag. 93 (2012) 883–898.
[10] K.Y. Yu, Y. Liu, C. Sun, H. Wang, L. Shao, E.G. Fu, X. Zhang, Radiation damage in helium ion irradiated nanocrystalline Fe, J. Nucl. Mater. 425 (2012) 140–146.
[11] M.J. Zhuo, E.G. Fu, L. Yan, Y.Q. Wang, Y.Y. Zhang, R.M. Dickerson, B.P. Uberuaga, A. Misra, M. Nastasi, Q.X. Jia, Interface-enhanced defect absorption between epitaxial anatase TiO_2 film and single crystal $SrTiO_3$, Scripta Mater. 65 (2011) 807–810.
[12] M.J. Zhuo, B.P. Uberuaga, L. Yan, E.G. Fu, R.M. Dickerson, Y.Q. Wang, A. Misra, M. Nastasi, Q.X. Jia, Radiation damage at the coherent anatase TiO_2/$SrTiO_3$ interface under Ne ion irradiation, J. Nucl. Mater. 429 (2012) 177–184.
[13] Z.X. Bi, B.P. Uberuaga, L.J. Vemon, J.A. Aguiar, E.G. Fu, S.J. Zheng, S.X. Zhang, Y.Q. Wang, A. Misra, Q.X. Jia, Radiation damage in heteroepitaxial $BaTiO_3$ thin films on $SrTiO_3$ under ne ion irradiation, J. Appl. Phys. 115 (2014) 124315.
[14] J. Li, K.Y. Yu, Y. Chen, M. Song, H. Wang, M.A. Kirk, M. Li, X. Zhang, In situ study of defect migration kinetics and self-healing of twin boundaries in heavy ion irradiated nanotwinned metals, Nano Lett. 15 (2015) 2922–2927.
[15] K. Kolluri, M.J. Demkowicz, R.G. Hoagland, X.Y. Liu, Behavior of vacancies and interstitials at semicoherent interfaces, JOM 65 (2013) 374–381.
[16] S.M. Mao, S.P. Shu, J. Zhou, R.S. Averback, S.J. Dillon, Quantitative comparison of sink efficiency of Cu–Nb, Cu–V and Cu–Ni interfaces for point defects, Acta Mater. 82 (2015) 328–335.
[17] M.J. Demkowicz, O. Anderoglu, X.H. Zhang, A. Misra, The influence of $\Sigma 3$ twin boundaries on the formation of radiation-induced defect clusters in nanotwinned Cu, J. Mater. Res. 26 (2011) 14.
[18] R.W. Siegel, S.M. Chang, R.W. Balluffi, Vacancy loss at grain boundaries in quenched polycrystalline gold, Acta Metall. 28 (1980) 249–257.
[19] T.C. Kaspar, M.E. Bowden, T. Varga, C.M. Wang, V. Shutthanandan, A.G. Joly, B.D. Wirth, R.J. Kurtz, Structural charactirization of epitaxial Cr_xMo_{1-x} alloy thin films, J. Phys. 24 (2012) 095001.
[20] C.M. Wang, T.C. Kaspar, V. Shutthanandan, A.G. Joly, L. Kovarik, B.W. Arey, M. Gu, A. Devaraj, B.D. Wirth, R.J. Kurtz, Structure and radiation damage behavior of epitaxial Cr_xMo_{1-x} alloy thin films on MgO, J. Nucl. Mater. 437 (2013) 55–61.
[21] Y. Xu, S.K. Yadav, J.A. Aguiar, O. Anderoglu, J.K. Baldwin, Y.Q. Wang, A. Misra, H.M. Luo, B.P. Uberuaga, N. Li, Irradiation-induced formation of a spinel phase at the FeCr/MgO interface, Acta Mater. 93 (2015) 87–95.
[22] J.H. Van Der Merwe, On the stresses and energies associated with inter crystalline boundaries, Proc. Phys. Soc. Lond. Sec. A 63 (1950) 616–637.
[23] J.H. Van Der Merwe, Crystal interfaces. Part I. Semi-infinite crystals, J. Appl. Phys. 34 (1963) 117–122.
[24] J.H. Van Der Merwe, Crystal Interfaces. Part II. Finite overgrowths, J. Appl. Phys. 34 (1963) 123–127.
[25] P. Tao, C. Zhang, Z.G. Yang, T. Hiroyuki, Evolution and coarsening of carbides in 2. 25Cr-1Mo steel weld metal during high temperature tempering, J. Iron Steel Res. Int. 17 (2010) 74–78.
[26] H. Lan, Z.G. Yang, Z.X. Xia, Y.D. Zhang, C. Zhang, Effect of dysprosium addition on the cyclic oxidation behaviour of CoNiCrAlY alloy, Corrosion Sci. 53 (2011) 1476–1483.
[27] E.G. Fu, Y. Fang, M.J. Zhuo, S.J. Zheng, Z.X. Bi, Y.Q. Wang, M. Tang, X. Ding, W.Z. Han, H.M. Luo, J.K. Baldwin, A. Misra, M. Nastasi, Interface structure of Nb films on single crystal MgO (100) and MgO (111) substrates, Acta Mater. 64 (2014) 100–112.
[28] V. Serin, S. Andrieu, R. Serra, F. Bonell, C. Tiusan, L. Calmels, M. Varela, S.J. Pennycook, E. Snoeck, M. Walls, C. Colliex, TEM and EELS measurements of interface roughness in epitaxial Fe-MgO-Fe magnetic funnel junctions, Phys. Rev. B 79 (2009) 144413.
[29] C. Wang, S.G. Wang, A. Kohn, R.C. Ward, A.K. Petford-Long, Transmission electron microscopy study of the Fe(001) vertical bar MgO(001) interface for magnetic tunnel junctions, IEEE Trans. Magn. 43 (2007) 2779–2781.
[30] I. Tanaka, M. Mizuno, S. Nakajyo, H. Adachi, Importance of metal–metal bondings at the interface of MgO and 3d-transition metals, Acta Mater. 46 (1998) 6511–6520.
[31] R.B. Marcus, Electrical and structural properties of epitaxial bcc tantalum films, J. Appl. Phys. 37 (1966) 3121–3126.
[32] C.M. Wang, T.C. Kaspar, V. Shutthahahdan, A.G. Joly, R.J. Kurtz, Structure of Cr film epitaxially grown on MgO(001), Acta Mater. 59 (2011) 4274–4282.
[33] Y. Ikuhara, P. Pirouz, S. Yadavalli, C.P. Flynn, Structure of V–MgO and MgO–V interfaces, Philos. Mag. A 72 (1995) 179–198.
[34] Y. Ikuhara, Y. Sugawara, I. Tanaka, P. Pirouz, Atomic and electronic structure of V/MgO interface, Interface Sci. 5 (1997) 5–16.
[35] K. Matsunaga, T. Sasaki, N. Shibata, T. Mizoguchi, T. Yamamoto, Y. Ikuhara, Bonding nature of metal/oxide incoherent interfaces by first-principles calculations, Phys. Rev. B 74 (2006) 125423.
[36] S.S. Perry, P.B. Merrill, Preparation and characterization of MgO(100) surfaces, Surf. Sci. 383 (1997) 268–276.
[37] S.A. Chamters, Epitaxial growth and properties of thin film oxides, Surf. Sci. Rep. 3 (2000) 105–180.
[38] J.J. Cuomo, J. Angilello, The growth of niobium on perfect and imperfect sapphire, J. Electrochim. Soc. 120 (1973) 125–128.
[39] K. Yoshii, H. Yamamoto, K. Saiki, A. Koma, Superconductivity and electrical properties in single-crystalline ultrathin Nb films grown by molecular beam epitaxy, Phys. Rev. B 52 (1995) 18.
[40] R. Benedek, D.N. Seidman, C. Woodward, The effect of misfit on heterophase interface energies, J. Phys. 14 (2002) 2877–2900.
[41] Y. Ikuhara, P. Pirouz, High resolution transmission electron microscopy studies of metal/ceramic interfaces, Microsc. Res. Tech. 40 (1998) 206–241.
[42] E.G. Fu, Y.Q. Wang, G.F. Zou, J. Xiong, M.J. Zhuo, Q.M. Wei, J.K. Baldwin, Q.X. Jia, L. Shao, A. Misra, M. Nastasi, Irradiation induced changes in small angle grain boundaries in mosaic Cu thin films, Appl. Phys. A 108 (2012) 121–126.
[43] R. Benedek, D.N. Seidman, M. Minkoff, L.H. Yang, A. Alavi, Atomic and electronic structure and interatomic potentials at a polar ceramic/metal interface:{222}MgO/Cu, Phys. Rev. B 60 (1999) 16094–16102.
[44] QuantumWise, Atomistix ToolKit(ATK) http://www.quantumwise.com.
[45] G.P. Stivastava, D. Weaire, The theory of the cohesive energies of solids, Adv. Phys. 36 (1987) 463–517.
[46] J.P. Perdew, A. Zunger, Self-interaction correction to density functional approximations for many-electron systems, Phys. Rev. B 23 (1981) 5048–5079.
[47] M.W. Finnis, The theory of metal-ceramic interfaces, J. Phys. 8 (1996) 5811.
[48] V. Gold, Compendium of Chemical Terminology, International Union of Pure and Applied Chemistry, in: A.D. McNaught, A. Wilkinson (Eds.), Blackwell Scientific Publications, Oxford, UK, 1987, p. 486.
[49] J.A. Dean, Lange's Handbook of Chemistry, 15th edition, McGraw-Hill, Inc., America, 1972, pp. 4.28–4.29.